Journal of Applied Remote Sensing

RemoteSensing.SPIEDigitalLibrary.org

Forest encroachment mapping in Baratang Island, India, using maximum likelihood and support vector machine classifiers

Laxmi Kant Tiwari
Satish K. Sinha
Sameer Saran
Valentyn A. Tolpekin
Penumetcha L. N. Raju

SPIE.

Forest encroachment mapping in Baratang Island, India, using maximum likelihood and support vector machine classifiers

Laxmi Kant Tiwari,[a,*] Satish K. Sinha,[a] Sameer Saran,[b] Valentyn A. Tolpekin,[c] and Penumetcha L. N. Raju[b]

[a]Rajiv Gandhi Institute of Petroleum Technology, Ratapur Chowk, Rae Bareli, Uttar Pradesh 229316, India

[b]Indian Space Research Organization, Indian Institute of Remote Sensing, 4-Kalidas Road, P.O. Box 135, Dehradun, Uttarakhand 248001, India

[c]University of Twente, Department of Earth Observation Science, P.O. Box 217, 7500 AE Enschede, The Netherlands

Abstract. Maximum likelihood classifier (MLC) and support vector machines (SVMs) are commonly used supervised classification methods in remote sensing applications. MLC is a parametric method, whereas SVM is a nonparametric method. In an environmental application, a hybrid scheme is designed to identify forest encroachment (FE) pockets by classifying medium-resolution remote sensing images with SVM, incorporating knowledge-base and GPS readings in the geographical information system. The classification scheme has enabled us to identify small scattered noncontiguous FE pockets supported by ground truthing. On Baratang Island, the detected FE area from the classified thematic map for the year 2003 was ~202 ha, and for the year 2013, the encroachment was ~206 ha. While some of the older FE pockets were vacated, new FE pockets appeared in the area. Furthermore, comparisons of different classification results in terms of Z-statistics indicate that linear SVM is superior to MLC, whereas linear and nonlinear SVM are not significantly different. Accuracy assessment shows that SVM-based classification results have higher accuracy than MLC-based results. Statistical accuracy in terms of kappa values achieved for the linear SVM-classified thematic maps for the years 2003 and 2013 is 0.98 and 1.0, respectively. © *2016 Society of Photo-Optical Instrumentation Engineers (SPIE)* [DOI: 10.1117/1.JRS.10.016016]

Keywords: forest encroachment; remote sensing; geographical information system; support vector machine; maximum likelihood classification.

Paper 15658 received Sep. 22, 2015; accepted for publication Jan. 21, 2016; published online Feb. 23, 2016.

1 Introduction

Natural disasters like floods, cyclones, drought, desertification, water scarcity, and soil erosion at large scales and their increasing frequency causing loss of human lives are being attributed to deforestation. The common driver for forest degradation and deforestation leading to such environmental problems is forest encroachment (FE).[1–5] The phrase "forest encroachment," or FE, was coined and legalized by the British Government in the Dean Forest (Encroachments) Act 1838 (1 and 2 Vict c 42). The Food and Agriculture Organization of the United Nations defined forest degradation as the reduction of the capacity of a forest to provide goods and services.[6] However, there is no globally approved definition for FE and forest degradation exist to date.[7] In India, the National Commission on Agriculture in 1976 considered FE a part of forest degradation and defined it as an unauthorized harvesting of forest produce and diversion of forest land to nonforest land use/land cover (LULC) practices, including "jhumming" (shifting cultivation). It is essential to maintain equilibrium in the biodiverse and fragile ecosystem; however, detecting and managing FE is an uphill task for any government or organization. Ever-increasing trends in

*Address all correspondence to: Laxmi Kant Tiwari, E-mail: lktiwari@rgipt.ac.in

1931-3195/2016/$25.00 © 2016 SPIE

the deforestation and degradation of forest must be reversed to save generations from their harmful effects.[8–12]

Environmental threats and impacts resulting from encroachments inside forested land, deforestation, forest degradation, and bad land use practices in the Andaman and Nicobar group of islands have been described in detail by several researchers.[13–17] The total forest cover of the island group is about 87% of its total geographical area.[18] A sudden increase in the population in the Andaman and Nicobar Islands during the 1970s resulted in increased FE, where people are largely dependent on the forests for their livelihood.[16,19] FE took place in remote areas in a concealed manner. Antiencroachment drives were not successful because of the inaccessibility of the remote FE areas, an inadequate number of forest officials, and a lack of political will. With the ever-increasing population and establishment of forest-based small-scale industrial units, there has been tremendous pressure on these natural forests, hence the problem of effective protection of forests has assumed greater importance, particularly to control illicit felling and encroachment on forest land. We have chosen Baratang Island, which is a part of the Andaman and Nicobar group of islands, to study FE in the area. It has several remotely located small noncontiguous FE pockets. The island has several landcover classes, which can be broadly divided into four classes: waterbody, mixed forest, mudflat, and builtup. The builtup class is a mixed landcover class that includes paddy field, house, bare soil and clay, and natural/planted trees. Monitoring of the class builtup is especially important, as periphery of the builtup area gradually expands with further encroachment.[20]

Remote sensing and a geographical information system (GIS) are powerful tools that help us in detecting FE due to their synoptic view to map large and small areas.[21] Using remotely sensed imagery, we get an updated and accurate map of geospatial features/targets in the form of LULC changes over large areas.[22–24] Furthermore, remote sensing provides data from inaccessible areas, repetitive coverage, and easy data acquisition at different scales and spatial resolutions.

Forest cover change or FE mapping has been performed using remote sensing and GIS in several studies.[25–29] Several digital image classification techniques are adopted to detect and map LULC classes from remote sensing data. These techniques can broadly be categorized into parametric, nonparametric, and visual interpretation. In many cases, different combinations of these techniques have provided better classification results.[25,26]

1.1 *Parametric Method*

In this statistical method of classification, a particular form of density distribution function (e.g., Gaussian) is assumed where statistical parameters for a class, such as mean and variance, need to be determined. As is true with any other statistical method, in this technique, the number of sample observations or training sites plays a crucial role in the estimation of statistical parameters. Examples of statistical classifiers based on parametric methods include maximum likelihood, Bayesian estimation, and stratified sampling, among others. These methods may lead to poor classification results in cases where the assumed distribution functions are not representative of the whole area under study. Some of the studies related to forest cover based on parametric methods are Assefa and Bork,[30] El-Tayeb et al.,[31] Kaoneka and Solberg,[32] Sunderlin and Resosudarmo,[33] Tiwari and Tolpekin,[34] and Tiwari et al.[20] Maximum likelihood classifier (MLC) is a commonly used and robust parametric method for LULC classification. When the data is normally distributed, MLC is an optimal choice wherein classification has a minimum overall probability of error.[35] However, accuracy of the thematic maps based on MLC is limited by the fact that the assumed characteristic distribution function may not be representative; it also lacks contextual information in its priori part among the pixels.[36–38] We have used MLC as the parametric classifier in this study and compared the results with those from support vector machine (SVM), which is a nonparametric classifier. The theoretical background of the MLC method is included as an Appendix A.

1.2 *Nonparametric Method*

Nonparametric classifiers, on the other hand, do not assume any statistical distribution function. Methods such as SVMs, artificial neural networks, nearest neighbor rule, fuzzy classification,

and kernel density estimation are nonparametric classifiers, which estimate distribution function based on training samples.[39] Such methods are important when there are overlapping classes and pixel values cannot be represented by a well-defined distribution function. Examples of nonparametric method–based studies to identify FE are Arekhi and Jafarzadeh,[40] Fauzi et al.,[41] and Mehdawi and bin Ahmad.[42] We have used SVM as the nonparametric method in our classification scheme.

Vapnik and Kotz[43] pioneered the SVM method and it is extensively used for signal processing in electrical engineering and other disciplines. However, it became popular in the field of remote sensing only about one-and-a-half decades ago.[44] Several studies in the field of remote sensing have been performed using SVMs.[45–53] A brief introduction to SVMs and relevant formulations is given as an Appendix A.

1.3 *Visual Interpretation Method*

Visual interpretation of a remote sensing image is a complex process of identifying objects based on tone, texture, shape, size, pattern, shadow, location, and association. In this technique, interpretation can be done on multiple false color composites of the same remotely sensed image with the help of photo interpretation key elements. In this type of technique, interpretation can be done by changing the band combinations of the multispectral data. In addition to that, it provides interpretation at the desired scale and allows us to apply various image enhancement techniques to extract information from the data. However, visual interpretation of FE is a subjective, time-consuming, and labor-intensive process, and it is also error prone.[20,54] Using the visual interpretation technique, we have selected training pixels to be used in parametric and nonparametric classification methods and evaluated the classified thematic maps.

1.4 *Hybrid Method*

Depending upon the types of data available, two or more methods can be combined in a hybrid approach; for example, parametric classifier and/or nonparametric classifier with knowledge-based methods. In a case study by Sastry et al.,[25] a hybrid method has been performed using interpretation enhancement techniques like lookup table stretch, histogram equalization, histogram match, haze reduction available in Erdas-Imagine software, and visual analysis to map FE in Manipur, India. Redowan et al.[28] studied forest cover change (or FE) using GIS with remotely sensed data. They used the normalized difference vegetation index and supervised classification method based on the density of forest cover to detect change over a period of 22 years. Kumari et al.[29] detected considerable change in the forest area using the remote sensing GIS technique with multitemporal satellite data.

In this study, we have compared LULC thematic maps of Baratang Island resulting from MLC and SVM. Distribution patterns of carefully selected training samples show deviation from a normal distribution. In such a case, we have chosen to use SVM as a nonparametric classification method. Different classes are well separated in feature space; therefore, SVM classification produced results with improved accuracy over MLC. Several other studies have also shown improvement in LULC classification with SVM when compared to other classifiers like MLC.[55–58] The objective of this study is to develop a hybrid scheme based on SVM classification with the aid of a knowledge base and GIS on the nominal scale of remotely sensed data to map FE. The hybrid method with recoding of few FE pockets has shown better classification results. However, small FE pockets in comparison to the spatial resolution of the test bed remotely sensed data could not be detected with SVM on a nominal scale.

2 Study Area and Data Used

Baratang Island is located between the latitudes of 12°8′N to 12°15′N and the longitudes of 92° 45′E to 92°53′E, covering an area of 29,760 ha. The island is a habitat of many endangered species, and the ecosystems of the island need to be protected from human impact.[19] The island has a typical wet tropical climate. Minimum and maximum mean temperatures during the last 3 years were recorded to be 24.5°C and 31°C, respectively, and the average annual precipitation was 3233 mm.[59] Baratang Island is one of the principal islands in the Baratang forest division.

The Baratang group of islands and Ritchie's Archipelago are separated by a channel (the Diligent Strait). Figure 1 shows a map of the study area. The entire landmass of this island is covered with luxuriant, almost impenetrable growth of tropical rain forest, characteristic of warm, humid, and wet tropics, except for the areas cleared for revenue settlements (the Government of India collects revenue from the inhabitants of these legalized settlements).

FE on the island over a decade is being studied using Indian Remote Sensing (IRS) satellite data from LISS-III sensors for the years 2003 and 2013. As given in Table 1, both IRS-1D and Resourcesat-2 have four spectral bands in the LISS-III sensors. All four spectral bands of Resourcesat-2 were used in the processing. However, the fourth band (i.e., B5) of IRS-1D could not be utilized in the image classification. The band B5 is full of strips, and destriping could not be performed, as the sensor details of IRS-1D LISS-III data are not provided to the users.

2.1 *Training and Validation Dataset*

Separate training data and accuracy assessment data were carefully selected from the IRS-1D LISS-III and Resourcesat2 LISS-III imagery for their respective years. For accuracy assessment, we took 560 pixels (140 pixels in each LULC class) from IRS-1D LISS-III images and 500 pixels (125 pixels in each class) from Resat2 LISS-III images. The areas for accuracy assessment were identified with the aid of visual assessment on the merged IRS-1C with PAN, with a 5.8-m spatial resolution for the year 2000, and on Resourcesat2 LISS-IV (5 m) for the year 2013 along with Google Earth data, ground truthing with GPS, and a knowledge base. A total of 1200 pixels (300 pixels for each LULC class) were selected for the training set in both image sets separately. An equal number of pixels in each class provides equal weight in the estimation of overall accuracy (OA). While selecting training data and accuracy assessment data, we ensured that the two did not intersect each other.

3 Methods

We have designed a hybrid method for digital classification of remotely sensed images for FE mapping [Figs. 2(a) and 2(b)]. In the first step, geometric and radiometric corrections were

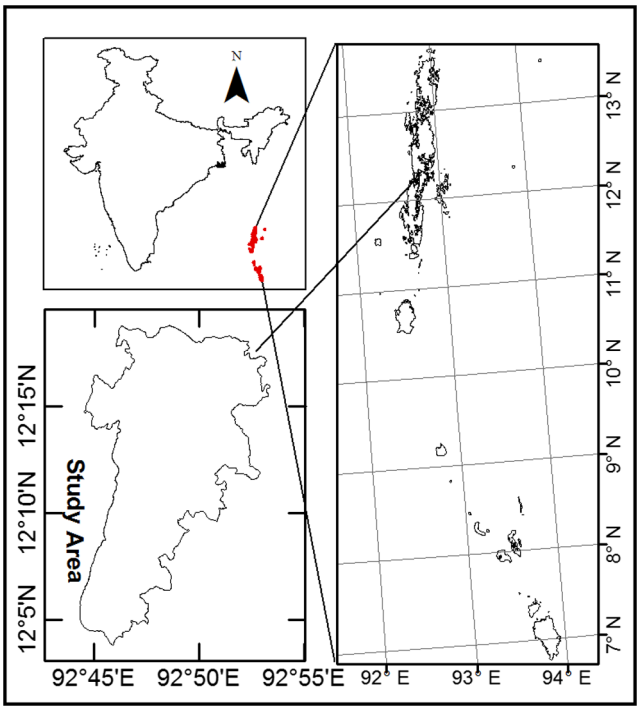

Fig. 1 Baratang Island is the study area, which is in the northern part of an archipelago including the Andaman and Nicobar Islands in the Indian Ocean.

Table 1 Remote sensing data used for the study is summarized here. All the data are from Indian remote sensing satellites.

Name of satellite/sensor	Date of acquisition	Spatial resolution	Spectral bands	
IRS-1D LISS-III	January 24, 2003	23.5 m		0.52 to 0.59 μm (B2) 0.62 to 0.68 μm (B3) 0.77 to 0.86 μm (B4)
IRS Resourcesat-2 LISS-III	February 5, 2013	23.5 m		0.52 to 0.59 μm (B2) 0.62 to 0.68 μm (B3) 0.77 to 0.86 μm (B4) 1.55 to 1.70 μm (B5)
IRS Resourcesat-2 LISS-IV	March 1, 2013	5.8 m		0.52 to 0.59 μm (B2) 0.62 to 0.68 μm (B3) 0.77 to 0.86 μm (B4)
IRS-1C – LISS-III-PAN merged data	February 14, 2000	5.8 m	IRS-1C – LISS-III	0.52 to 0.59 μm (B2) 0.62 to 0.68 μm (B3) 0.77 to 0.86 μm (B4)
			IRS-1C PAN	0.50 to 0.75 μm

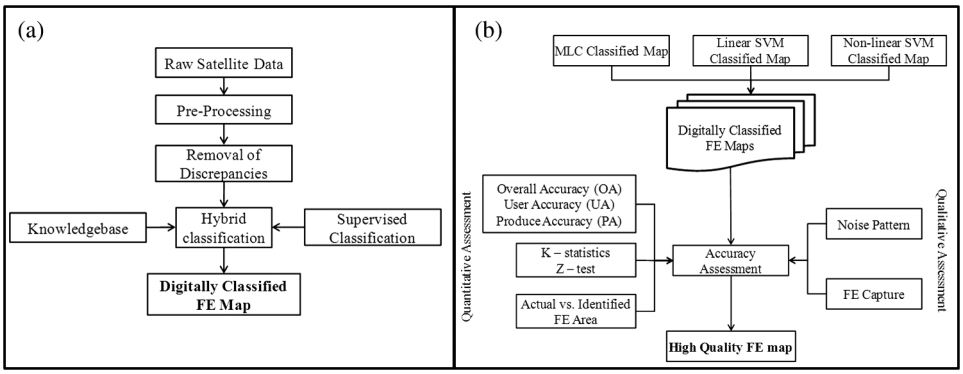

Fig. 2 (a) The hybrid method followed to produce digitally classified FE maps. (b) Steps involved in qualitative and quantitative accuracy assessment of the classified FE maps.

applied to the raw satellite data, followed by removal of discrepancies (e.g., haze removal). In the next step, a hybrid classification scheme, i.e., supervised classification (MLC/SVM), combined with the knowledge base, was implemented on the test bed data. While qualitative accuracy of different classes is assessed with the help of high-resolution imagery including Google Earth, statistical parameters, such as κ-statistics, Z-test, user accuracy (UA), and producer accuracy (PA), are estimated for quantitative assessment.

The knowledge base was obtained from geospatial data (i.e., high-resolution remotely sensed images, topographical maps, and village maps) and nongeospatial data (i.e., interviews and field visits). Interactions with the Andaman and Nicobar Forest Department (ANFD), local institutions (revenue department), and field officers (i.e., expert knowledge) associated with FE were also made for updating the knowledge base.

In the image classification process, training and validation datasets for the Resourcesat-2 LISS-III and IRS-1D LISS-III images were created using a random pixel selection strategy, which guarantees maximum variation and representativeness available for each class.[60] The training set consisted of four classes, namely mudflat, mixed forest, waterbody, and builtup. The target FE is close to the class builtup. It should be noted that the builtup class is a mixed land cover class composed of harvested paddy field, house/hut, natural and planted trees, wet/dry soil, and clay. In the case of class mudflat, it was very difficult to get pure training pixels, as it also contains bare/wet/dry soil, clay, and sand. In the medium-resolution images of LISS-III, getting pure pixels of the builtup and mudflat classes was even more challenging. Since

the number of pixels in the classes acts as weight in the estimation of OA, equal numbers of homogeneous pixels for each LULC class were selected. IRS-1C LISS-III merged with PAN and Resourcesat-2 LISS-IV high-resolution images (Fig. 3) were used as a visual aid/guide when selecting training pixels and validation polygons.

We have implemented MLC- and SVM-based image classification by writing codes in R, a free software environment for statistical computing and graphics.[61] The "kernlab" package is used for the SVM method, and the "k-SVM" function is used for both linear and nonlinear SVM with optimal hyperparameters.

4 Results

4.1 *Application of Maximum Likelihood Classifier*

MLC is a parametric classifier that takes into account the mean and covariance of the input data to classify it into an output thematic map. Normality tests of various classes in different bands using Q-Q plots do not show normal distribution except for the mixed forest class in the near infrared (NIR) band (Figs. 4 and 5). This is expected because of higher reflectivity from vegetation in the NIR band. We have applied MLC on the input remotely sensed data and compared the results with the SVM results. It should be noted that while nonintersecting training and validation datasets are prepared separately for different images, they are not changed for different classification algorithms.

4.2 *Application of Support Vector Machine*

We have used SVM as a nonparametric classifier. Both linear and nonlinear SVMs have been used to classify the remote sensing images, and the output thematic maps are compared among themselves as well as with MLC-based thematic maps. Feature space plots of training datasets are shown in Figs. 6 and 7. Visibly, waterbody and mixed forest are linearly separable, while builtup and mudflat show some overlap. In case of nonlinear SVM, a Gaussian radial basis function (RBF) kernel has been used on all test bed multispectral remotely sensed images. The performance of SVM is affected by the kernel functions, and the behavior of SVM with different types of kernel functions has been investigated by various researchers.[57,62,63]

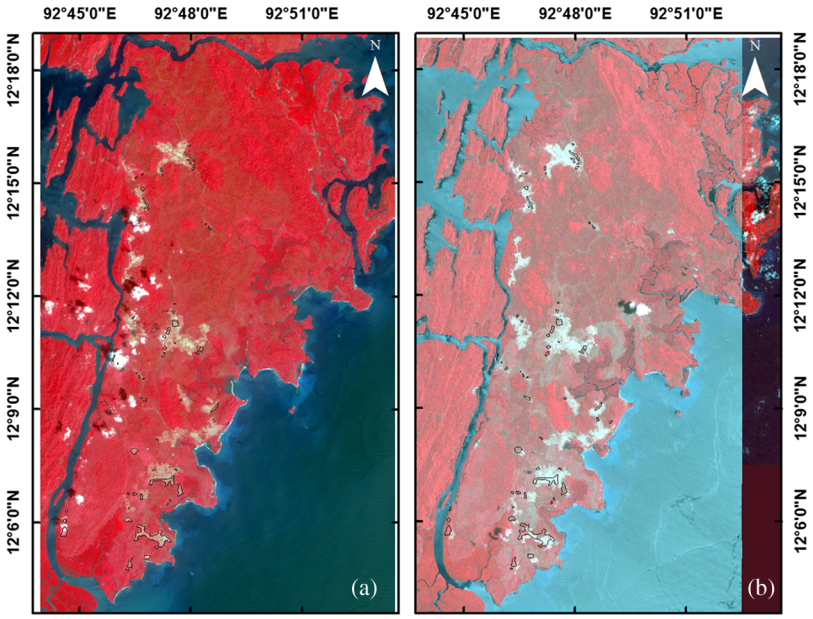

Fig. 3 (a) False color image (RGB:321) of Resourcesat-2 LISS-IV (5.8 m) for the year 2013 and (b) IRS-1C LISS-III image for the year 2000 merged with PAN (5.8 m) data.

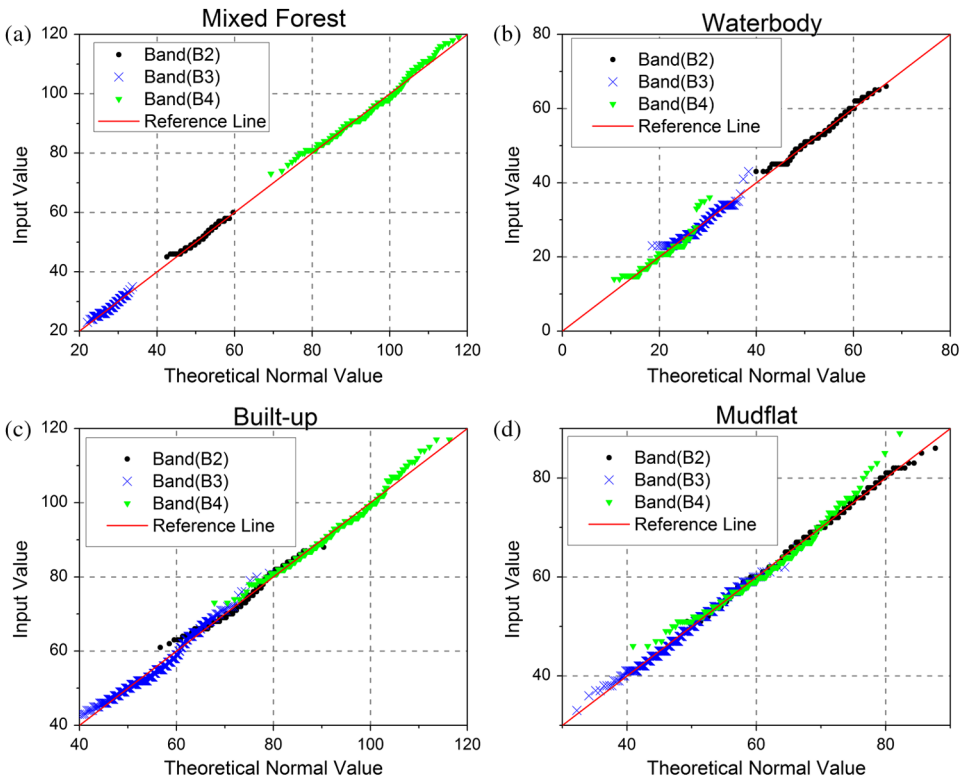

Fig. 4 *Q-Q* plots of training pixels for different classes. Different bands are represented in different colors. A reference line is drawn to show deviation from normal distribution. The data are from an IRS-1D LISS-III image from the year 2003. Details of the spectral bands are given in Table 1. (a) Mixed forest; (b) waterbody; (c) builtup; and (d) mudflat.

Right optimization of the hyperparameters (C and σ) associated with RBF leads to better performance of SVM. Theoretical background and details on the optimization of hyperparameters are given in the Appendix A.

A tuning set with all the LULC classes was used to obtain an optimal range of the hyperparameters. In the next step, we optimize hyperparameters for the linear case (i.e., C) and the nonlinear case (i.e., C and σ) by assessing qualitative and quantitative results of the validation dataset. Using these values of hyperparameters, we have classified the study area test bed of remotely sensed images. The optimal values of C and σ for the RBF kernel are 1 and 0.3, respectively, for the classification of Resourcesat-2 LISS-III images. For the classification of IRS-1D LISS-III images, the optimal values of hyperparameters are $C = 1$ and $\sigma = 0.6$.

4.3 *Classification of Resourcesat-2 LISS-III Image for the Year 2013*

Output thematic maps of the MLC classifier and of the two SVM classifiers are shown in Figs. 8(a)–8(c). Qualitative investigation of the results suggests that SVM outperformed MLC. The southern part of Baratang Island is enlarged in Fig. 9 to show that the classification results of MLC are nosier and separations of FE pockets are not good in comparison to the classification results of SVMs. Comparison of linear and nonlinear SVM results [Figs. 9(b) and 9(c)] shows that the nonlinear SVM overdetected mudflat areas and the builtup class in some places. However, FE pockets in both SVMs show negligible change. There are 56 FE pockets on the island, covering an area of 210 ha. SVM detected 1.9% less than the actual FE, whereas MLC overdetected FE by 16.6% (Table 2). These results are further assessed quantitatively and compared in terms of UA, PA, and OA.[20] A comparison of MLC, linear SVM, and nonlinear SVM results in terms of accuracy parameters derived from confusion matrices for different classes is shown in Table 3. The classification map from linear SVM has the highest accuracy.

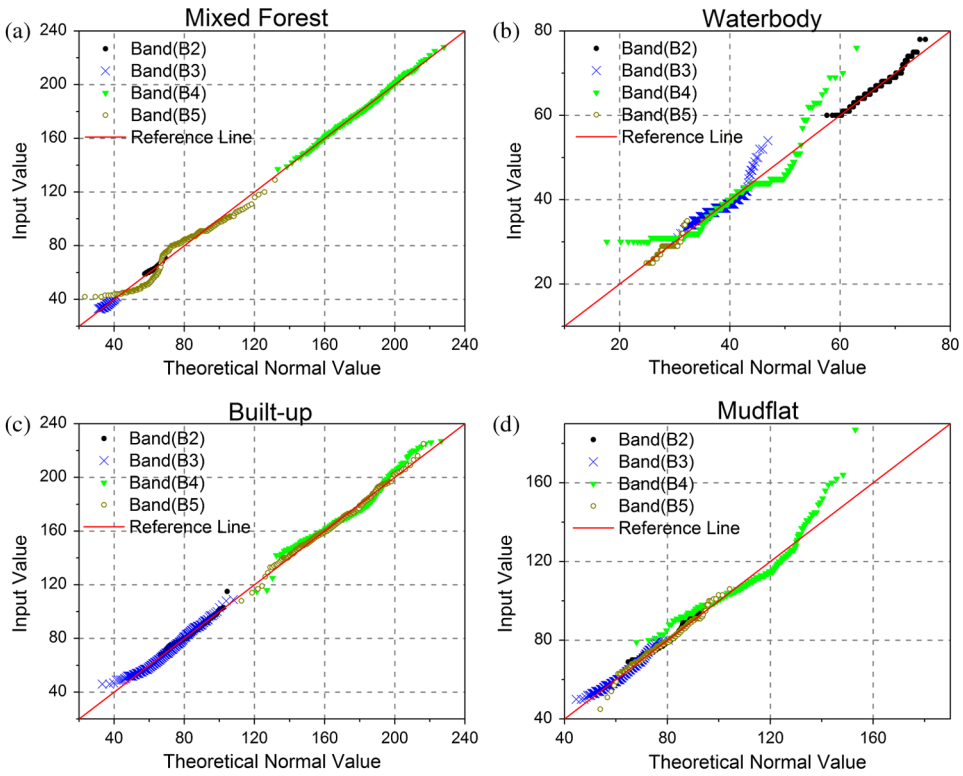

Fig. 5 The data for *Q-Q* plots from Resat-2 LISS-III (year 2013). Different bands of training pixels are plotted in different colors. Deviation from a reference line shows non-normal distribution. Spectral details of different bands are given in Table 1. (a) Mixed forest; (b) waterbody; (c) builtup; and (d) mudflat.

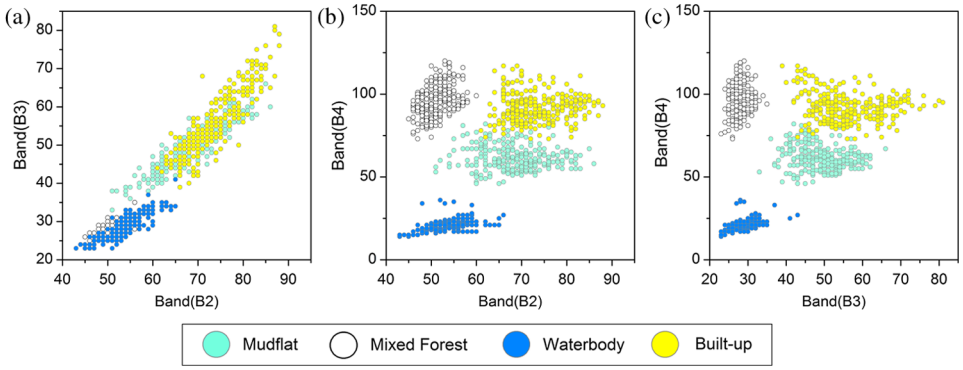

Fig. 6 Three bands of IRS-1D LISS-III (i.e., B2, B3, and B4) for the training set are plotted in the feature space. (a) B2 versus B3; (b) B2 versus B4; (c) B3 versus B4.

Furthermore, we calculated kappa (κ) statistics for each map and performed the Z-test to compare two different classified maps (Table 4).[64,65] The statistical results indicate that while linear and nonlinear SVM classified maps are similar in the 95% confidence interval (i.e., with probability of significance of 1.645), both of them are significantly better than the MLC classified map. Thus, SVM performance was superior to MLC for FE mapping in our area. The FE pocket polygons overlaid on the classified maps [Figs. 8(a)–8(c)] were constructed from the Resourcesat-2 LISS-IV (5 m) data, GPS readings, and the knowledge base [Fig. 3(a)]. It should be noted that each FE pocket in the study area was visited to capture its GPS reading. The FE areas of the GPS polygons were in agreement with the data provided by ANFD.

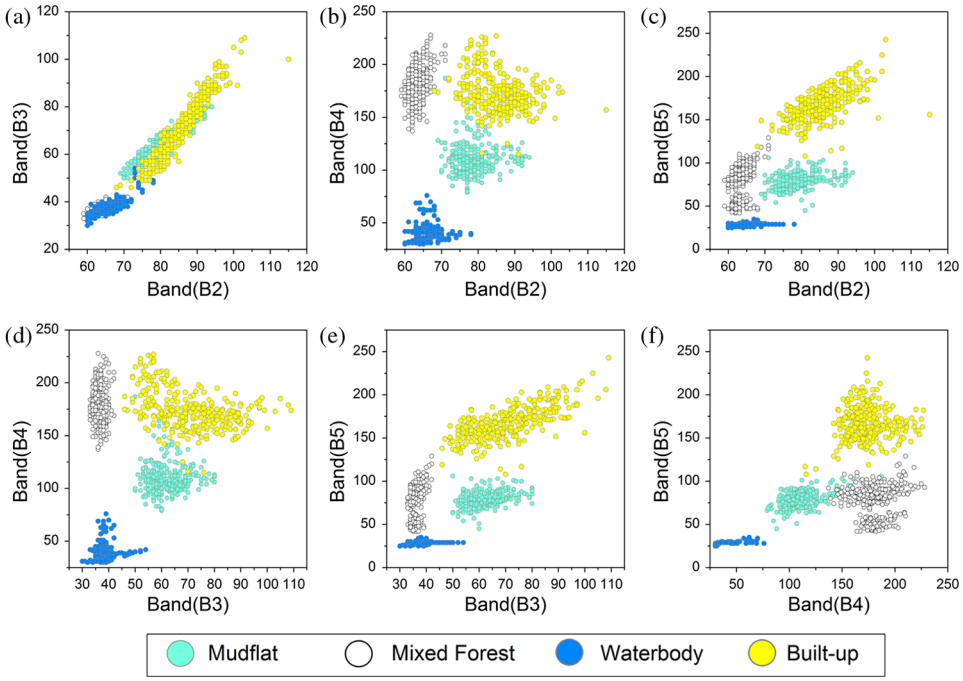

Fig. 7 Four bands of Resourcesat-2 LISS-III (i.e., B2, B3, B4, and B5) for the training set are plotted in the feature space. (a) B2 versus B3; (b) B2 versus B4; (c) B2 versus B5; (d) B3 versus B4; (e) B3 versus B5; (f) B4 versus B5.

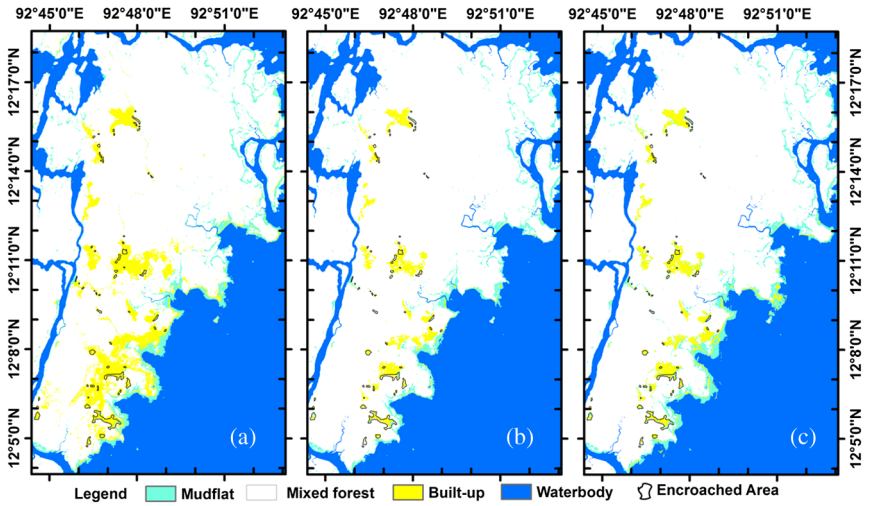

Fig. 8 Output thematic maps for the year 2013 based on (a) MLC, (b) linear SVM, and (c) nonlinear SVM. Polygons on the thematic maps show encroached area.

4.4 *Classification of IRS-1D LISS-III Images for the Year 2003*

The resultant images of the MLC and SVM classifiers on the test bed of the IRS-1D LISS-III data are shown in Figs. 10(a)–10(c). Separation of small FE pockets in the classified images of SVMs is evidently better than that of the MLC classified images. Furthermore, MLC classified images appear nosier than SVM (both linear and nonlinear) classified maps, as seen in Fig. 10. The southern part of Baratang Island is enlarged in Fig. 11 to compare the noise pattern in the classified images. We observe that SVMs output better classification maps qualitatively as compared to MLC for the year 2003 as well.

Quantitative assessments of the two methods for image classification are given in Table 5. MLC has falsely detected 8.97% more FE, whereas only 4.71% of the FE area remained

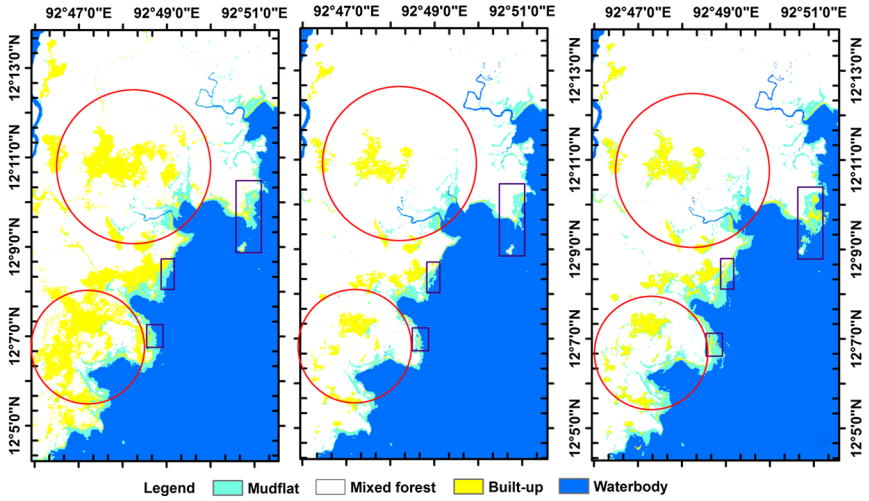

Fig. 9 Output thematic maps showing southern part of Baratang Island using (a) MLC, (b) linear SVM, and (c) nonlinear SVM. Encircled areas show presence of noise in MLC thematic map. Boxed areas show overdetection with nonlinear SVM classification.

Table 2 Quantitative comparison between SVM and MLC classified maps, 2013.

		Area (in Ha) detected by		Difference in area (in %) detected by	
Number of FE pockets	Area (Ha)	MLC	Linear SVM	MLC	Linear SVM
56	210	245	206	16.6 (+)	1.9 (–)

Table 3 User accuracy (UA), producer accuracy (PA), and overall accuracy (OA) derived from confusion matrix of SVM and MLC classified maps, 2013.

	MLC		Linear SVM		Nonlinear SVM	
OA	95		100		99	
Class	UA (%)	PA (%)	UA (%)	PA (%)	UA (%)	PA (%)
Mudflat	100.0	99.2	100.0	100.0	99.2	99.2
Mixed forest	100.0	82.4	100.0	100.0	100.0	100.0
Waterbody	100.0	100.0	100.0	100.0	100.0	100.0
Builtup	84.4	100.0	100.0	100.0	99.2	100.0

Table 4 κ- and Z-statistics for MLC and SVM classified maps, 2013.

κ-statistics	MLC	Linear SVM	Nonlinear SVM
	0.93	1.00	0.99
Z-statistics	Linear versus MLC	Nonlinear versus MLC	Linear versus nonlinear
	$\|Z\| = 4.9$	$\|Z\| = 4.3$	$\|Z\| = 1.42$

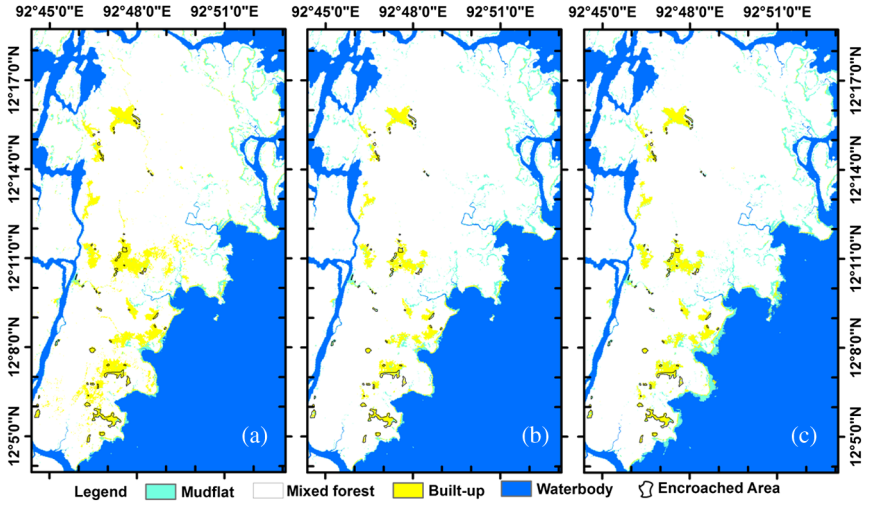

Fig. 10 Output thematic maps for the year 2003 based on (a) MLC, (b) linear SVM, and (c) nonlinear SVM. Polygons on the thematic maps show encroached area.

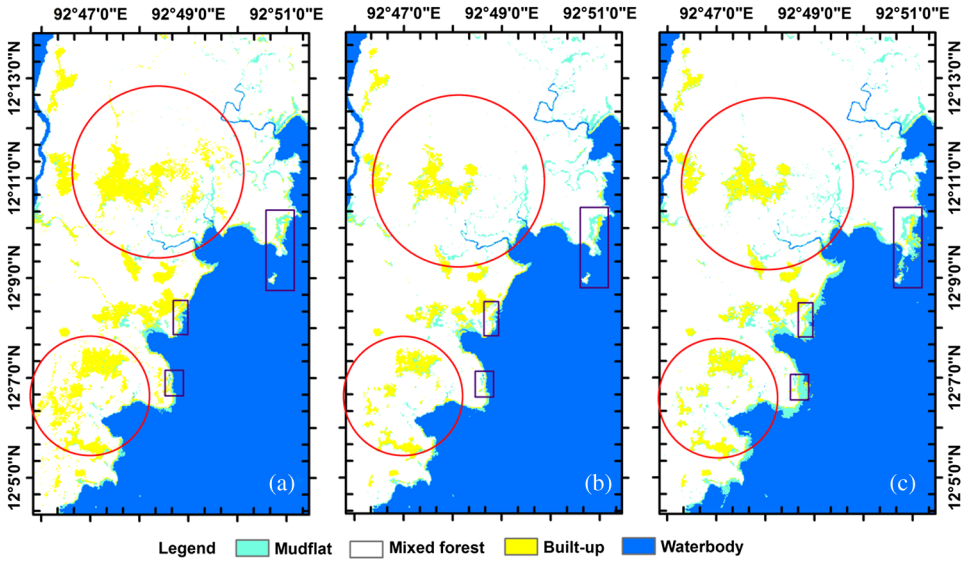

Fig. 11 Southern part of Fig. 10 zoomed in. The classification maps are based on: (a) MLC, (b) linear SVM, and (c) nonlinear SVM. Encircled areas show presence of noise in MLC thematic map. Boxed areas show overdetection with nonlinear SVM classification.

Table 5 Quantitative comparison between linear SVM and MLC classified maps for the year 2003.

		Area (in Ha)detected by		Difference in area (in %) detected by	
Number of FE pockets	Area (Ha)	MLC	Linear SVM	MLC	Linear SVM
55	212	231	202	8.97 (+)	4.71 (–)

undetected by linear SVM. Note that the FE area for the year 2003 and its location are provided by ANFD. Furthermore, extensive fieldwork with GPS was conducted to corroborate the area of FE pockets in the study area. Statistical accuracy for different classified maps, as summarized in Table 6, shows that SVM has an edge over MLC when compared in terms of OA. UA in the confusion matrix for SVM, in comparison with MLC, has significantly improved in the case of

Table 6 UA, PA, and OA derived from confusion matrix of SVM and MLC classified maps, 2003.

	MLC		Linear SVM		Nonlinear SVM	
OA	97		99		98	
Class	UA (%)	PA (%)	UA (%)	PA (%)	UA (%)	PA (%)
Mudflat	97.0	95.0	97.8	97.8	98.5	95.0
Mixed forest	100.0	97.6	100.0	100.0	100.0	100.0
Waterbody	100.0	100.0	100.0	100.0	100.0	100.0
Builtup	93.1	97.1	97.8	97.8	95.1	98.5

class builtup, which matches the FE. Performance based on statistical measures of SVMs and MLC for image classification is shown in Table 7. Although linear SVM has a higher value of kappa (κ), there is no significant difference between the three maps in terms of Z-statistics in the 95% confidence interval.

Using the classification scheme based on linear SVM, the change in the builtup class area is studied from the thematic maps of the years 2003 and 2013. In Figs. 12(a) and 12(b), the observed changes are circled. In the northwestern part of Fig. 12, encroached forested land has now been vacated by the encroachers after the tsunami in 2004. The encroachment is clearly seen on the same spot of Fig. 12(a). A photograph taken during the field visit is shown in Fig. 13(a). The picture shows a mudflat in front of planted coconut and arecanut trees and an emptied and imperceptible structure on the left. Two newer FE pockets are observed on the maps, one in the southern part and another in the eastern part of Fig. 12, which resulted in an increase of FE during the year 2013 in comparison to year 2003. Figures 13(b) and 13(c) are snapshots from the southern FE pocket. One can see a newly built house, planted coconut and arecanut trees, cattle grazing the field, and straw and stubble in the field. Figure 13(d) is a snapshot from the eastern FE pocket. A simple tin shade structure is seen in the backdrop of the arable area. Also, there appears to be an increase in the mudflat area in the post-tsunami period, as evident in the eastern part of Fig. 12.

5 Discussion

Remote sensing–based FE mapping on Baratang Island is supported by extensive fieldwork that was conducted with handheld GPS, visiting and identifying each FE pocket in the study area. GPS reading polygons were overlaid on the images in a GIS environment. An expert knowledge base and departmental data on FE were incorporated to outline each FE pocket.

Out of the four different LULC classes (mudflat, mixed forest, waterbody, and builtup), changes in the builtup area between classified images from 2003 and 2013 has been used as a proxy for FE, supported by field visits and the knowledge base. The randomly picked training dataset had only 1.2% pixels for the IRS-1D LISS-III as unknown, and only 0.75% pixels for the Resourcesat-2 LISS-III were recognized as unknown. Out of the four classes, waterbody and

Table 7 κ- and Z-statistics for MLC and SVM classified maps, 2003.

κ-statistics	MLC	Linear	Non-linear
	0.96	0.98	0.97
Z-statistics	Linear versus MLC	Nonlinear versus MLC	Linear versus nonlinear
	$\|Z\| = 1.81$	$\|Z\| = 1.05$	$\|Z\| = 0.78$

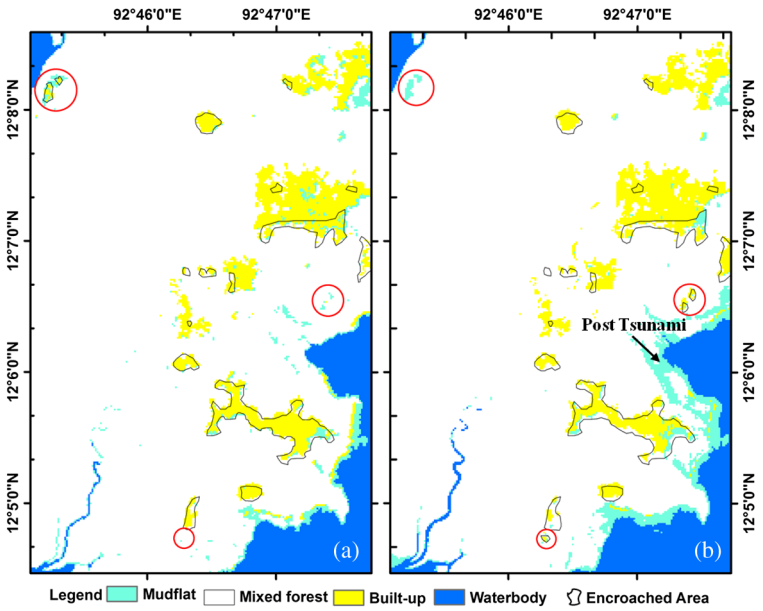

Fig. 12 Part of SVM classified maps to show change in FE between (a) 2003 and (b) 2013. Changes are encircled in both maps for comparison. Polygons on the thematic maps show encroached area.

mixed forest are classified with 100% accuracy, which is due to high spectral discrimination capabilities for these particular classes, as seen in Figs. 6 and 7. In the feature space, they are separable in bands B2, B3, and B4. Also, bands B2 and B4 have spectral values close to normal distribution for mixed forest and waterbody (Figs. 4 and 5). It is important to note that the vegetation reflects almost half of the NIR (band B4 in this case) back into the atmosphere. In the case of dense forest, one would expect multiple atmospheric scattering of reflected NIR radiation contaminating the values from the clearings (i.e., FE). In our study, however, spectral characteristics of the builtup area and the forested area are well separated in the

Fig. 13 These snapshots were taken in the year 2014. The snapshot (a) is from the area that had been vacated after the tsunami in 2004 (upper left encircled area in Fig. 12). The snapshots (b) and (c) are new FEs corresponding to the encircled area in the southern part of Fig. 12. The snapshot (d) is new FE corresponding to the encircled area in the eastern part of Fig. 12.

feature space (Figs. 6 and 7), resulting in FE mapping with high accuracy. Mixed pixels resulting from increasing forest density and decreasing FE size would reduce the accuracy of FE mapping with this method. This study ignored the adjacency effect related to atmospheric scattering but still managed to get reasonably high classification accuracy.

In general, builtup and mudflats have less accuracy compared to mixed forest and waterbody. Furthermore, we observe that in case of MLC, the UA of the class mudflat is higher for the LISS-III image in 2013 compared to that for the LISS-III image in 2003 (Tables 3 and 6). This could be a result of the fact that four bands (i.e., B2, B3, B4, and B5) in the larger spectral range of Resourcesat-2 LISS-III have been used in the classification, whereas only three bands (i.e., B2, B3, and B4) of the LISS-III sensor of IRS-1D were useful in the image classification. The separability of the class mudflat improves with the inclusion of band B5, as seen in the B2 to B5 and B3 to B5 feature spaces (Fig. 7). A detailed analysis of confusion matrices shows that it is due to confusion of builtup with wetland, and wetland is confused with mixed forest with complex and close boundaries. The UA of the builtup and mudflat classes in SVM is better than that in MLC.

While application of MLC on the normally distributed class with Gaussian distribution brings better results, the particular probability distribution of the class is irrelevant in the case of SVM. In both SVM and MLC classified maps, some noise is observed because the mudflat and builtup classes have large variance. MLC maps are noisier in comparison with SVM maps. It is pertinent to mention here that both test bed images were captured by the sensors in the postharvest period. In Andaman and Nicobar Islands, paddy is harvested before January 15 of each year. Hence, there is no paddy present in the field; it is open. However, at several places, the field is covered by straw or very small grasses. There are few and scattered locations of houses in the builtup area, occupying only a small amount of ground in comparison to the paddy field. In addition to that, there are natural forested trees inside the builtup area. Nonetheless, we have successfully identified FE pockets located in the study area. The FE area provided by ANFD matches with our field data. The statistical accuracy of the linear and nonlinear SVM classifications for both years, i.e., 2003 and 2013, outperformed the MLC classifier. Comparison of the thematic maps for the year 2013 in terms of Z-test also suggests that while linear and nonlinear SVM results have the same proportions, they are somewhat different from MLC results. The small difference between linear and nonlinear SVM (Tables 4 and 7) may be attributed to random selection of accuracy assessment sites. Thus, in our application of mapping FE, SVM proves to be a better classifier than MLC qualitatively and quantitatively. In a few places, FE pockets were only partially detected, as they are too small with respect to the spatial resolution of the remotely sensed images. We have the limitation of using high-resolution images, which is beyond the scope of this study. The SVM classifier produced higher accuracy ($\sim$1%) for thematic maps based on Resourcesat-2 compared to those based on IRS-1D. This could be attributed to the number of spectral bands used and the radiometric resolution of the sensors. Resourcesat-2 LISS-III images have four bands with 10 unsigned bit radiometric resolution, whereas IRS-1D LISS-III images have three bands with 8 unsigned bit radiometric resolution. Additional separability is provided by the inclusion of band B5 and is evident from the values of the SVM hyperparameters. The RBF kernel for the year 2013 images has a smaller standard deviation compared to that for the 2003 images, while the cost parameter remains the same ($\sigma = 0.3$ for Resourcesat-2 images and $\sigma = 0.6$ for IRS-1D images).

6 Conclusions

In this study, the commonly used image classification methods of MLC and SVM were implemented with a knowledge base to identify FE in Baratang Island of the Andaman and Nicobar group of islands, India. The classification performance of linear and nonlinear SVMs was compared with MLC. A comparison study based on Z-statistics reveals that while linear SVM is significantly better than MLC, linear and nonlinear SVM results are not significantly different. Due to their spectral separability compared to other LULC classes, forest and waterbody were classified with high accuracy. In our classification scheme, while the waterbody class includes creek and sea water, the forest class consists of tropical evergreen and semievergreen forest

types. The study shows that SVM is more effective in FE mapping than MLC. Integration of the knowledge base with SVM-classified thematic maps played an important role in proper identification of FE. Thus, the hybrid scheme that has been developed in this study paves the path for similar studies in small or large areas.

The study shows that effective implementation of such a classification scheme has many implications toward mapping and monitoring of land cover change, especially for small patches using coarse/medium resolution satellite images. Also, such an approach when operationalized can be used to effectively map and monitor the trees outside forests over large regions, which is a challenging issue at present. FE at the individual level is not investigated and is beyond the scope of this study. However, by adopting the scheme developed in this study, one can implement it over a larger area for identification of FE.

Appendix A: Theoretical Background

A1 Maximum Likelihood Classification

MLC is a widely used supervised statistical classification method in remote sensing. It assigns a given pixel to a specific class based on the conditional probability concept. The likelihood for a given pixel with spectral value $\mathbf{x}$ to be of class ω_i is determined using Bayes's theorem and is represented as $p(\omega_i|\mathbf{x})$. The maximum likelihood decision rule for each pixel in the remotely sensed image under MLC is calculated by the natural logarithm of likelihood or "discriminant function"[38] given by

$$g_i(\mathbf{x}) = \ln\{p(\mathbf{x}|\omega_i)p(\omega_i)\} = \ln\ p(\mathbf{x}|\omega_i) + \ln\ p(\omega_i), \tag{1}$$

where $p(\omega_i)$ is the prior probability of the i'th class ω_i, and $\mathbf{x}$ represents a column vector of the brightness value for the pixel in the multispectral bands.

Classification of pixels is based on the probability that a pixel falls within a certain class. MLC finds the probability of a pixel belonging to a particular class based on a certain threshold value. Each pixel is assigned to the class that has the highest probability (i.e., the maximum likelihood). If the highest probability is smaller than the specified threshold value, the pixel remains unclassified.

The "discriminant function" shown in Eq. (1) is a general form of MLC with respect to a probability density function. Commonly, the multivariate normal distribution function, also known as Gaussian distribution, is assumed for the data in each class of the multispectral remotely sensed images. The probability density function for Gaussian distribution in $\mathbf{N}$-dimensional space is given as

$$p(\mathbf{x}|\omega_i) = (2\pi)^{-N/2}\ |\mathbf{C}_i|^{-1/2} \exp\{-1/2(\mathbf{x}-\mathbf{m}_i)^{\mathrm{T}}\mathbf{C}_i^{-1}(\mathbf{x}-\mathbf{m}_i)\}, \tag{2}$$

where $\mathbf{C}_i$ and $\mathbf{m}_i$ are the covariance matrix and mean vector of the data, respectively, in the i'th class. Substituting Eq. (2) into Eq. (1) and omitting the class independent term gives the discriminant function as[38,66]

$$g_i(\mathbf{X}) = \ln\ p(\omega_i) - \frac{1}{2}\ \ln|\mathbf{C}_i| - \frac{1}{2}(\mathbf{x}-\mathbf{m}_i)^{\mathrm{T}}\mathbf{C}_i^{-1}(\mathbf{x}-\mathbf{m}_i). \tag{3}$$

A2 Support Vector Machine

SVM is a supervised nonparametric statistical classification method to classify multispectral images. It started as a binary classifier in which an optimal hyperplane is constructed with a maximized margin that separates all training vectors into two classes labeled as $+1$ and -1.[36] Training samples that lie on the margins of decision boundaries are called the support vectors. Depending on the distribution and separability of training data in the feature space, linear or nonlinear SVM is used for classification.

A2.1 *Linear Support Vector Machine Classification*

A2.1.1 *Linear-separable case*

Suppose that there are N numbers of a training dataset represented by $\{\mathbf{x}_i, y_i\}, i = 1, \ldots, N, y_i \in \{1, -1\}, \mathbf{x}_i \in \mathbf{R}^{\mathrm{d}}$. Here, $\mathbf{x}_i$ is the observed multispectral features and y_i is its class label.[36] A linear hyperplane in feature space is defined as

$$\mathbf{w} \cdot \mathbf{x}_i + b = 0, \tag{4}$$

where $\mathbf{x}$ is a point lying on the hyperplane, $\mathbf{w}$ is normal to the hyperplane, and b indicates the bias. For a linearly separable case, the separating hyperplane can be defined for two classes as

$$y_i(\mathbf{w} \cdot \mathbf{x}_i + b) \geq 1, \quad \text{for all } y_i = +1 \quad \text{and} \quad y_i = -1. \tag{5}$$

The margin between the two canonical hyperplanes is $2/\|\mathbf{W}\|$. In order to maximize the margin, $\mathbf{w}$ needs to be minimized. It is a nonlinear optimization task and can be achieved by $\min\{\frac{1}{2}\|\mathbf{W}\|^2\}$ with Lagrange multipliers[38] using the constraints as in Eq. (5).

A2.1.2 *Linear nonseparable case*

When the classes are not linearly separable from each other, the soft margin method can be employed for classification of samples with minimal errors.[36,67] An optimal solution is achieved by introducing a slack variable ξ in the optimization procedure as

$$\min\left[\frac{\|\mathbf{W}\|^2}{2} + C\sum_{i=1}^{N}\xi_i\right], \tag{6}$$

where C is a penalty or cost parameter. The first part is used to maximize the margin and the cost parameter C is used to penalize the training vectors situated on the wrong side of the decision boundary.[36] C is essentially a tradeoff between errors of the SVM on the training data and margin maximization subject to constraints:[68]

$$y_i(\mathbf{w} \cdot \mathbf{x}_i + b) \geq 1 - \xi_i, \xi_i \geq 0, i = 1, \ldots, N. \tag{7}$$

A2.2 *Nonlinear Support Vector Machine Classification*

A nonlinear SVM algorithm is used when a linear hyperplane with either a hard or soft margin cannot separate the classes. The feature space is mapped into a higher dimensional space to improve separation between classes. The training set ($\mathbf{x}_i \in R^n$) is projected into a higher dimensional space (H) using a nonlinear mapping function: Φ: $R^n \rightarrow H$.[67]

A vector $\mathbf{x}$ in the feature space is introduced as $\Phi(\mathbf{x})$ in H. A scalar product of the transformed feature is used as a kernel function and is written as[57]

$$K(\mathbf{x}_i, \mathbf{x}_j) = \Phi(\mathbf{x}_i) \cdot \Phi(\mathbf{x}_j). \tag{8}$$

Details of SVM formulation for linear and nonlinear separability can be found in Richards[38] and Tso and Mather.[36]

There are several kernel functions used in SVM that are categorized as linear, polynomial, RBF, and sigmoid kernel. However, polynomial and RBF are commonly used kernels in remote sensing for digital image classification.[53,57,58,69] In this study, we have used the Gaussian RBF kernel $K(\mathbf{x}_i, \mathbf{x}_j) = \exp(-\|\mathbf{x}_i - \mathbf{x}_j\|^2/2\sigma^2)$ to map the input data into nonlinear feature space. σ is a hyperparameter of the RBF kernel function, also known as kernel

width.[69] The algorithm is implemented with a soft margin. The performance of SVMs varies depending on the proper optimization of the kernel parameter σ and the cost parameter C. The optimal value of σ usually lies between the range of 0.1 and 0.9 quantile of $\|\mathbf{x}_i - \mathbf{x}_j\|$ statistics.[70,71]

Acknowledgments

We thank the director of RGIPT and the director of IIRS for supporting this research work. We would like to thank Shri Omkar Singh, IFS, PCCF/Principal Secretary, ANI Forest Department for allowing us to visit the study area and for providing ancillary data to accomplish this study. We would also like to thank the Divisional Forest Officer, Baratang, for his support and help during the field visit. We appreciate Shri Keshabanand Ganguly, field officer (survey and settlement camp, Baratang Forest Division) for identifying and showing us FE pockets and for his tireless efforts. We thank the range officers of Nilambur and Adazig along with their field staff and officials. We would like to thank ACF along with all the executive staff of GIS Cell/ANSAC, Van Sadan, for providing data and ancillary information on FE. We also thank Raymond Hunt, associate editor of *Journal of Applied Remote Sensing*, and the reviewers for their valuable comments and suggestions.

References

1. J. Alcamo and E. M. Bennett, and Millennium Ecosystem Assessment (Program), *Millennium Ecosystem Assessment: Ecosystem and Human Well-Being: A Framework for Assessment*, Island Press, Washington, DC (2003).
2. K. S. Rao and R. Pant, "Land use dynamics and landscape change pattern in a typical micro watershed in the mid elevation zone of Central Himalaya, India," *Agric. Ecosyst. Environ.* **86**(2), 113–124 (2001).
3. M. C. Hansen, S. V. Stehman, and P. V. Potapov, "Quantification of global gross forest cover loss," *Proc. Natl. Acad. Sci.* **107**(19), 8650–8655 (2010).
4. R. Sarmah, "Non-timber forest products and their utilization pattern in Changlang district of Arunachal Pradesh," PhD Thesis, Rajiv Gandhi University, Itanagar, India (2006).
5. G. B. Bonan, "Forests and climate change: forcings, feedbacks, and the climate benefits of forests," *Science* **320**(5882), 1444–1449 (2008).
6. FAO, *Expert Meeting on Harmonizing Forest-Related Definitions for Use by Various Stakeholders*, Intergovernmental Panel on Climate Change, Rome, Italy (2002).
7. FAO, "Assessing forest degradation, towards the development of globally applicable guidelines," in *Forest Resources Assessment Working Paper 177*, p. viii + 99, Food and Agriculture Organization of the United Nations, Rome (2011).
8. A. Dai, "Drought under global warming: a review," *Wiley Interdiscip. Rev. Clim. Change* **2**(1), 45–65 (2011).
9. O. E. Sala et al., "Global biodiversity scenarios for the year 2100," *Science* **287**(5459), 1770–1774 (2000).
10. P. M. Fearnside, "Global warming and tropical land-use change: greenhouse gas emissions from biomass burning, decomposition and soils in forest conversion, shifting cultivation and secondary vegetation," *Clim. Change* **46**(1–2), 115–158 (2000).
11. A. de Sherbinin et al., "Population and environment," *Annu. Rev. Environ. Resour.* **32**, 345–373 (2007).
12. F. Achard et al., "Determination of deforestation rates of the world's humid tropical forests," *Science* **297**(5583), 999–1002 (2002).
13. N. P. Balakrishnan, "Andaman Islands—vegetation and floristics," in *Andaman, Nicobar and Lakshadweep: An Environmental Impact Assessment*, Oxford Publishing Company, New Delhi, India (1989).
14. P. Pande et al., *Directory of National Parks and Sanctuaries in Andaman and Nicobar Islands: Management Status and Profiles*, Centre for Public Policy, Planning and Environmental Studies, Indian Institute of Public Administration, New Delhi, India (1991).

15. W. A. Rodgers and S. H. Panwar, *Biogeographical Classification of India*, New Forest, Dehradun, India (1988).
16. C. J. Saldanha, *Andaman, Nicobar and Lakshadweep: An Environmental Impact Assessment*, Oxford University Press, New Delhi (1989).
17. Z. Whitaker, "The Jarawa tribals—a cry for survival," *India Mag.* **5**, 64–71 (1985).
18. FSI, *India State of Forest Report 2013*, p. 252, Forest Survey of India, Dehradun, India (2013).
19. C. J. Saldanha et al., *Andaman and Nicobar Islands: An Environmental Impact Assessment*, Ministry of Environment and Forests Government of India, Bangalore, India (1987).
20. L. K. Tiwari et al., "Markov random field-based method for super-resolution mapping of forest encroachment from remotely sensed ASTER image," *Geocarto Int.* **31**(4), 428–445 (2016).
21. K. A. Ulbricht and W. D. Heckendorff, "Satellite images for recognition of landscape and landuse changes," *ISPRS J. Photogramm. Remote Sens.* **53**(4), 235–243 (1998).
22. T. N. Carlson and G. A. Sanchez-Azofeifa, "Satellite remote sensing of land use changes in and around San José, Costa Rica," *Remote Sens. Environ.* **70**(3), 247–256 (1999).
23. J. P. Guerschman et al., "Land cover classification in the Argentine Pampas using multi-temporal Landsat TM data," *Int. J. Remote Sens.* **24**(17), 3381–3402 (2003).
24. Z. Dezso et al., "Analysis of land-use/land-cover change in the Carpathian region based on remote sensing techniques," *Phys. Chem. Earth, Parts A/B/C* **30**(1–3), 109–115 (2005).
25. K. L. N. Sastry et al., "Nationwide forest encroachment mapping using remote sensing and GIS technique—Manipur state," Final Technical Report, p. 92, Manipur Forest Department, Imphal (2007).
26. G. R. P. Kumar et al., "Assessment of forest encroachment at Belgaum district of Western Ghats of Karnataka using remote sensing and GIS," *J. Environ. Biol.* **35**, 259–264 (2014).
27. K. V. Satish et al., "Geospatial assessment and monitoring of historical forest cover changes (1920-2012) in Nilgiri Biosphere Reserve, Western Ghats, India," *Environ. Monit. Assess.* **186**(12), 8125–8140 (2014).
28. M. Redowan, S. Akter, and N. Islam, "Analysis of forest cover change at Khadimnagar National Park, Sylhet, Bangladesh, using Landsat TM and GIS data," *J. For. Res.* **25**(2), 393–400 (2014).
29. M. Kumari et al., "Change detection analysis using multi temporal satellite data of Poba reserve forest, Assam and Arunachal Pradesh," *Int. J. Geomatics Geosci.* **4**(3), 517–525 (2014).
30. E. Assefa and H. R. Bork, "Deforestation and forest management in Southern Ethiopia: investigations in the Chencha and Arbaminch areas," *Environ. Manage.* **53**(2), 284–299 (2014).
31. I. El-Tayeb, A. Bishay, and H. Dregne, "A bioenergy project to reduce deforestation in Sudan," in *Second Int. Desert Development Conf.* pp. 225–229, Harwood Academic Publishers, Cairo, Egypt (1991).
32. A. R. S. Kaoneka and B. Solberg, "Forestry related land use in the West Usambara mountains, Tanzania," *Agric. Ecosyst. Environ.* **49**(2), 207–215 (1994).
33. W. Sunderlin and I. A. P. Resosudarmo, "The effect of population and migration on forest cover in Indonesia," *J. Environ. Dev.* **8**(2), 152–169 (1999).
34. L. K. Tiwari and V. A. Tolpekin, "Effectiveness of markov random field based method for super-resolution mapping from satellite images to investigate forest encroachment," in *100th Indian Science Congress*, pp. 52–53, Indian Science Congress Association, Kolkata, India (2013).
35. S. M. Davis et al., *Remote Sensing: The Quantitative Approach*, Vol. **1**, p. 405, McGraw-Hill International Book Co., New York (1978).
36. B. Tso and P. Mather, *Classification Methods for Remotely Sensed Data*, 2nd ed., CRC Press, Taylor & Francis Group, Boca Raton, Florida (2009).
37. D. A. Landgrebe, *Signal Theory Methods in Multispectral Remote Sensing*, John Wiley & Sons, Inc., Hoboken, New Jersey (2005).
38. J. Richards, *Remote Sensing Digital Image Analysis: An Introduction*, 5th ed., Springer, Heidelberg (2013).

39. Y. Kumar and G. Sahoo, "Analysis of parametric & non parametric classifiers for classification technique using WEKA," *Int. J. Inf. Technol. Comput. Sci.* **4**(7), 43–49 (2012).
40. S. Arekhi and A. A. Jafarzadeh, "Forecasting areas vulnerable to forest conversion using artificial neural network and GIS (case study: northern Ilam forests, Ilam province, Iran)," *Arabian J. Geosci.* **7**(3), 1073–1085 (2014).
41. A. Fauzi, Y. A. Hussin, and M. Weir, "A comparison between neural networks and maximum likelihood remotely sensed data classifiers to detect tropical rain logged-over forest in Indonesia," in *22nd Asian Conf. on Remote Sensing*, pp. 616–621, CRISP, Singapore (2001).
42. A. A. Mehdawi and B. bin Ahmad, "Classification of forest change by integration of remote sensing data with neural network techniques," in *Int. Conf. on System Engineering and Technology (ICSET)*, pp. 1–5 (2012).
43. V. N. Vapnik and S. Kotz, *Estimation of Dependences Based on Empirical Data*, Springer-Verlag, New York (1982).
44. G. Mountrakis, J. Im, and C. Ogole, "Support vector machines in remote sensing: a review," *ISPRS J. Photogramm. Remote Sens.* **66**(3), 247–259 (2011).
45. G. M. Foody, "RVM-based multi-class classification of remotely sensed data," *Int. J. Remote Sens.* **29**(6), 1817–1823 (2008).
46. B. Dixon and N. Candade, "Multispectral landuse classification using neural networks and support vector machines: one or the other, or both?," *Int. J. Remote Sens.* **29**(4), 1185–1206 (2008).
47. A. B. Salberg and R. Jenssen, "Land-cover classification of partly missing data using support vector machines," *Int. J. Remote Sens.* **33**(14), 4471–4481 (2012).
48. N. Kausar, A. Majid, and M. Sattar, "A novel ensemble scheme for the multi-focus image fusion using support vector machine," *Int. J. Comput. Math.* **91**(9), 2072–2090 (2014).
49. B. Zheng et al., "A support vector machine to identify irrigated crop types using time-series Landsat NDVI data," *Int. J. Appl. Earth Obs. Geoinf.* **34**, 103–112 (2015).
50. G. B. Scofield, E. Pantaleao, and R. G. Negri, "A comparison of accuracy measures for remote sensing image classification: case study in an Amazonian region using support vector machine," *Int. J. Image Proc.* **9**(1), 11–21 (2015).
51. A. De Giorgi, G. Moser, and S. B. Serpico, "Contextual remote-sensing image classification through support vector machines, Markov random fields and graph cuts," in *IEEE Int. Geoscience and Remote Sensing Symp.*, pp. 3722–3725 (2014).
52. Y. Chun et al., "SVM method used to study gender differences based on microelement," *Phys. Proc.* **33**, 212–215 (2012).
53. T. Kavzoglu and I. Colkesen, "A kernel functions analysis for support vector machines for land cover classification," *Int. J. Appl. Earth Obs. Geoinf.* **11**(5), 352–359 (2009).
54. J. Miettinen, H. J. Stibig, and F. Achard, "Remote sensing of forest degradation in Southeast Asia—aiming for a regional view through 5–30 m satellite data," *Global Ecol. Conserv.* **2**, 24–36 (2014).
55. G. M. Foody and A. Mathur, "Toward intelligent training of supervised image classifications: directing training data acquisition for SVM classification," *Remote Sens. Environ.* **93**(1–2), 107–117 (2004).
56. G. M. Foody et al., "Training set size requirements for the classification of a specific class," *Remote Sens. Environ.* **104**(1), 1–14 (2006).
57. C. Huang, L. S. Davis, and J. R. G. Townshend, "An assessment of support vector machines for land cover classification," *Int. J. Remote Sens.* **23**(4), 725–749 (2002).
58. M. Pal and P. M. Mather, "Support vector machines for classification in remote sensing," *Int. J. Remote Sens.* **26**(5), 1007–1011 (2005).
59. GOI, "A&N at A Glance 2015 handbook," (2015) http://www.and.nic.in/
60. T. Kavzoğlu, "Determination of environmental degradation due to urbanization and industrialization in Gebze, Turkey," *Environ. Eng. Sci.* **25**(3), 429–438 (2008).
61. R Foundation, "The R Project for Statistical Computing," (2015) https://www.r-project.org/
62. B. Schölkopf et al., "Comparing support vector machines with Gaussian kernels to radial basis function classifiers," *IEEE Trans. Signal Process.* **45**(11), 2758–2765 (1997).

63. I. Steinwart, "On the influence of the kernel on the consistency of support vector machines," *J. Mach. Learn. Res.* **2**, 67–93 (2002).
64. R. G. Congalton and K. Green, *Assessing the Accuracy of Remotely Sensed Data*, CRC Press, London (2008).
65. E. Raymond Hunt, Jr., J. H. Gillham, and C. S. T. Daughtry, "Improving potential geographic distribution models for invasive plants by remote sensing," *Rangeland Ecol. Manage.* **63**(5), 505–513 (2010).
66. A. Asmala and S. Quegan, "Analysis of maximum likelihood classification on multispectral data," *Appl. Math. Sci.* **6**(129), 6425–6436 (2012).
67. C. Cortes and V. Vapnik, "Support-vector networks," *Mach. Learn.* **20**(3), 273–297 (1995).
68. M. Rychetsky, *Algorithms and Architectures for Machine Learning Based on Regularized Neural Networks and Support Vector Approaches*, Shaker, Shaker Verlag GmbH, Berlin, Germany (2001).
69. S. S. Keerthi and C. J. Lin, "Asymptotic behaviors of support vector machines with Gaussian kernel," *Neural Comput.* **15**(7), 1667–1689 (2003).
70. A. Karatzoglou, D. Meyer, and K. Hornik, "Support vector machines in R," *J. Stat. Software* **15**(9), 1–28 (2006).
71. B. Caputo et al., "Appearance-based object recognition using SVMs: which Kernel should I use?," in *Proc. of NIPS Workshop on Statistical Methods for Computational Experiments in Visual Processing and Computer Vision*, Whistler (2002).

Laxmi Kant Tiwari is pursuing his doctoral studies in geoinformatics at RGIPT, Rae Bareli, India. He received his bachelor's and master's degrees in computer applications from IGNOU, New Delhi, in 2004 and 2007, respectively. He graduated with a master's in geoinformatics from ITC, University of Twente, The Netherlands, in 2011. He has been a forester with the Department of Environment and Forests in Andaman and Nicobar Islands since 2003.

Satish K. Sinha is currently an associate professor at Rajiv Gandhi Institute of Petroleum Technology at Rae Bareli. He received his MSc degree in applied geology from IIT Kharagpur, India, in 1998 and his PhD in geophysics from the University of Oklahoma in 2006. His research interests include geophysical signal processing and interpretation.

Sameer Saran is scientist and head, Geoinformatics Department, Indian Institute of Remote Sensing (Indian Space Research Organisation), Dehradun, India. He received his PhD in geoinformatics. His present area of interest is 3-D city modeling, WebGIS, advanced geospatial modeling and health GIS, and so on. He has published around 70 papers in peer-reviewed journals. He is recipient of many awards like Indian National Geospatial Award, ISRO Bhuvan Team Excellence Award, ASI Team, ESRI Best paper award, and so on.

Valentyn A. Tolpekin received his MSc degree in theoretical physics from Odessa State University, Odessa, Ukraine, in 1975. He obtained his PhD at the University of Twente in physics in 2004. He is currently an assistant professor at the Department of Earth Observation Science, ITC. His research interests focus on mathematical and statistical tools for satellite image analysis, including Markov random fields, super-resolution mapping, and support vector machines.

Penumetcha L. N. Raju is scientist "G" and director at North Eastern Space Applications Centre, Department of Space, Government of India. He received his BE degree in civil engineering from Mysore University and MTech in remote sensing from Anna University in 1984 and 1987, respectively. He is the author of more than 45 journal papers and contributor of in-house GIS book publication of IIRS. His current research interests include geoinformatics, remote sensing applications, 3-D GIS, and visualization. He is a member of scientific societies in India (i.e., ISRS, ISG, INCA, IASWC, and IMS).